Infrared–optical double resonance spectroscopy of the NH 2 radical

Takayoshi Amano, Kentarou Kawaguchi, Masao Kakimoto, Shuji Saito, and Eizi Hirota

Citation: The Journal of Chemical Physics **77**, 159 (1982); doi: 10.1063/1.443663
View online: http://dx.doi.org/10.1063/1.443663
View Table of Contents: http://scitation.aip.org/content/aip/journal/jcp/77/1?ver=pdfcov
Published by the AIP Publishing

Infrared–optical double resonance spectroscopy of the NH_2 radical

Takayoshi Amano,[a] Kentarou Kawaguchi, Masao Kakimoto,[b] Shuji Saito, and Eizi Hirota

Institute for Molecular Science, Okazaki 444, Japan
(Received 19 January 1982; accepted 17 March 1982)

Vibration-rotation transitions of NH_2 in the $\tilde{A}\,^2A_1$ state were observed with sub-Doppler resolution, by using a Rh 6G dye laser and a CO_2/N_2O laser combined with the laser magnetic resonance technique. When the dye laser pumped the $\tilde{A}\,^2A_1$ (0,9,0) $2_{20}\leftarrow\tilde{X}\,^2B_1$(0,0,0) 1_{10} transition, 39 M_J components of (0,10,0) $2_{11}\leftarrow$(0,9,0) 2_{20}, and 5 M_J components of (0,10,0) $1_{11}\leftarrow$(0,9,0) 2_{20} in $\tilde{A}$ were observed by sweeping the magnetic field. Four additional lines which corresponded to changes in fluorescence intensity opposite in sign to those for the transitions mentioned above, were also observed and assigned to transitions from $\tilde{A}\,^2A_1$(0,9,0) to a highly excited vibrational state of $\tilde{X}$ ("u" level). The rotational quantum numbers N and J and the spin splitting of the u level were determined as well as the interaction term between the u and $\tilde{A}$(0,10,0) 2_{11} states. The u level is tentatively assigned to a rotational level in $\tilde{X}$(2,8,0), however, the observed spin splitting does not agree with that for $\tilde{X}$(0,8,0) calculated by Jungen, Hallin, and Merer.

I. INTRODUCTION

The double resonance technique has been proved to be powerful in observing very weak transitions, particularly in the excited electronic or vibrational states, in unambiguously assigning complicated spectra, and in studying collisional relaxation processes. Among various combinations of radiation sources, few examples, however, have been reported on double resonance experiments with an infrared laser and a visible or ultraviolet laser as radiation sources. A double resonance experiment with a cw CO_2 laser and a cw Ar^+ laser was carried out on NO_2.[1] The double resonance technique with a pulsed CO_2 and a pulsed UV laser was applied to D_2CO and HDCO.[2] However, no high-resolution sub-Doppler spectroscopy with IR–visible or IR–UV double resonance seems to have been reported.

We have applied the infrared–visible double resonance technique to NH_2 to explore vibration-rotation transitions in the excited electronic state with high resolution. One of the advantages of infrared–visible and visible–visible double resonance is that excited electronic states which are otherwise forbidden to reach, or difficult to access due to unfavorable Franck–Condon factor, from the ground state by a single-step process can be observed. In this experiment either a visible laser or an infrared laser with narrow linewidth selectively excites a Doppler component and the other laser monitors the resultant hole burning, giving sub-Doppler signals. The linewidth of the infrared signals observed on pumping a visible transition by a dye laser can be almost as narrow as the homogeneous linewidth, as will be shown later. On the other hand, the double resonance signal observed by sweeping a visible transition is not as narrow as a homogeneous linewidth because of an incomplete compensation for the Doppler width, but it still has a much narrower linewidth than the Doppler width.

The NH_2 molecule is one of the most thoroughly investigated free radicals in the gas phase. Dressler and Ramsay[3] have made an extensive analysis of the visible bands recorded by flash photolyzing NH_3. Johns, Ramsay, and Ross[4] have extended the measurements to longer wavelengths and improved the molecular constants. More recently, absorption and laser induced fluorescence spectra were further extensively examined to obtain high precision spectroscopic data as well as information on dynamical behavior of the molecule.[5–10] For the ground vibronic state, far-infrared laser magnetic resonance (FIR LMR) has provided very accurate molecular constants.[11] Curl and his collaborators performed a series of elaborate experiments of microwave–optical double resonance (MODR).[12–16] They concentrated their observations mainly on rotational transitions in the ground electronic state, but several rotational transitions in the excited electronic state were also measured. Kawaguchi *et al.* observed the LMR spectra of the ν_2 fundamental band in the ground electronic state with a CO laser as a source.[17] They analyzed their data combined with those from the FIR LMR and from the MODR experiments to derive even more accurate molecular constants. Further improvement of the molecular parameters was recently made through a combined analysis of all the available data from the optical to the microwave regions.[18]

In the excited $\tilde{A}$ electronic state of the NH_2 free radical, the fundamental bending vibration frequency is about 630 cm^{-1}. However, the shape of the potential function for the HNH bending is closer to a quartic rather than a quadratic potential with a shallow hump at the center. As a result, the vibrational spacing between the $v_2=9$ and $v_2=10$ states increases to about 920 cm^{-1}. Transitions from the ground vibronic state to the $\tilde{A}$(0, 9, 0) or $\tilde{A}$(0, 10, 0) vibronic states appear in the very convenient range of a dye laser with Rh 6G. Therefore, high-resolution vibration-rotation spectroscopy in the excited electronic state is feasible with CO_2 and N_2O lasers in conjunction with the technique of laser magnetic resonance, when the visible transitions are pumped by a dye laser. Information on the hyperfine splittings in a few rotational states of the $\tilde{A}$(0, 9, 0) and $\tilde{A}$(0, 10, 0) vibronic

[a] Present address: Herzberg Institute of Astrophysics, National Research Council of Canada, Ottawa, Ontario, Canada K1A 0R6. Permanent address: Department of Physics, University of Tokyo, Hongo, Tokyo 113, Japan.

[b] Present address: Technical Research Center, Komatsu Ltd., 2597 Shinomiya, Hiratsuka, Kanagawa 254, Japan.

 0021-9606/82/130159-09$02.10

states has already been provided by saturation spectroscopy[19] and by level-crossing spectroscopy.[20] The narrow infrared linewidth expected for the IR–visible double resonance experiment will, however, enable us to observe further resolved hyperfine structures in the excited vibronic states. Incorporation of the LMR technique may cause complications in the observed spectra, but will provide us with information on the g factors in the excited states through precise analyses of the observed Zeeman shifts.

II. EXPERIMENTAL

A. Apparatus

Figure 1 shows a schematic diagram of the experimental setup. The cell was placed inside a CO_2/N_2O infrared laser cavity. The visible laser beam from a dye laser (CR 599-21) with Rh 6G solution was introduced into the cell through the end concave mirror made of ZnSe for the infrared laser. About a quarter of the visible laser power was passed through the ZnSe mirror. In some experiments the cell was placed outside the infrared laser cavity by moving the end reflector of the infrared laser to the place indicated by M' in the figure.

The intracavity arrangement required no stringent alignment of the two laser beams. The visible laser beam was weakly focused, and the beam spot size at the center of the cell was about 5 mm. On the other hand, in the case of the extra-cavity cell configuration, the infrared laser was focused at the midpoint between the centers of the pole caps of the magnet in order to increase the power density. As a result, the dye laser beam was also focused at the same point. The beam waist was estimated to be less than 1 mm for both beams. The S/N ratio of a line with a fairly large infrared transition moment was better for the intracavity than for the extra-cavity arrangements, mainly because the number of molecules subjected to both the laser beams at the same time and involved in the double resonance process was much larger in the former than in the latter arrangement. The extra-cavity cell configuration was used for the detection of weak infrared transitions such as the "u" lines, as shown below, because the power density is an order of magnitude larger in the extra-cavity system than in the intracavity system.

The output power of the dye laser was about 80 mW. The frequency of the dye laser was approximately set by using a Spex 14018 double monochromator, and was measured more accurately by recording the fluorescence spectrum of I_2. The visible spectrum was recorded with frequency markers at every 1.5 GHz or 150 MHz derived from temperature-stabilized etalons.[21]

The infrared laser used was of conventional design; each oscillation line could be selected by rotating a grating mounted at an end of the laser cavity. The output power was about 500 mW for the CO_2 to 10 μm $P(6)$ line and about 150 mW for the N_2O $R(20)$ line. The oscillation frequency was carefully stabilized by adjusting the voltage applied to the piezoelectric translator.

The fluorescence observation cell, which formed a part of the gas flow system, was placed between the

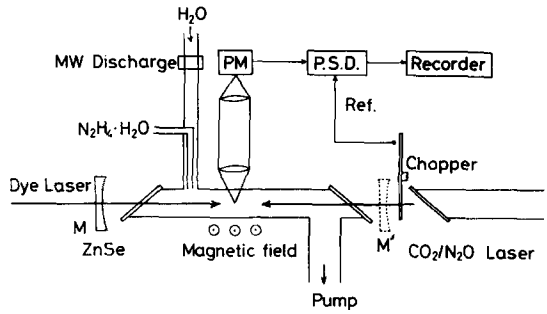

FIG. 1. Block diagram of the infrared–optical double resonance spectrometer with an intracavity cell. In an extracavity experiment, the end mirror M of the infrared laser was moved to the place indicated by M'.

pole faces of a Varian 15" electromagnet. Any combination of the polarization of the visible and the infrared lasers relative to the magnetic field could be selected by using a polarization rotator for the visible laser and by rotating the Brewster windows and grating for the infrared laser. The magnetic field strength was calibrated by observing proton or deuteron magnetic resonance signals. The uncertainty of the field measurement was about 10 G and the hyperfine splitting of one M_J component was measured with the accuracy of a few G.

The infrared laser light was chopped at 690 Hz by a mechanical chopper. Fluorescence was collected through a telescope on a photomultiplier (HTV R712) placed well outside the magnet so that it was unaffected by the magnetic field. The signal was processed with a lock-in amplifier (PAR 124A) at the chopping frequency. Therefore, only the change in the intensity of the fluorescence brought about by infrared irradiation was detected.

A suitable interference filter was used in most observations. For example, in observing the $\tilde{A}(0, 10, 0)2_{11} - \tilde{A}(0, 9, 0)2_{20}$ infrared transition, a band-pass filter centered at 568 nm with a full width of 10 nm was employed. The wavelengths of the fluorescence from the $\tilde{A}(0, 10, 0)2_{11}$ level to the 1_{01}, 2_{21}, and 3_{21} rotational levels of the ground vibronic state are 569, 572, and 574 nm, respectively. Other vibronic bands from the $\tilde{A}(0, 10, 0)$ state to the excited vibrational states in the ground electronic state, which are located in the wavelength region longer than 615 nm, are much weaker than those to the ground vibronic state. The shortest wavelength fluorescence from the $\tilde{A}(0, 9, 0)2_{20}$ state lies at about 598 nm. Therefore, the use of the filter permitted us to detect almost exclusively the fluorescence from the $\tilde{A}(0, 10, 0)$ vibronic state without any significant loss, and gave the double resonance signal as an increase in the fluorescence intensity. Another merit of using the filter is that the scattering of dye laser light used as pumping radiation can be suppressed almost completely.

The NH_2 free radicals were produced by the reaction of hydrated hydrazine with microwave discharged products in H_2O. The sample pressure was estimated to be about 40–60 mTorr. The reaction conditions such as the partial pressures of the constituent vapors and the

flow rate were optimized by monitoring the laser induced fluorescence of NH_2.

B. Observation of the signals

The vibration-rotation transition frequencies in the excited $\tilde{A}$ electronic state were calculated using the term values given by Dressler and Ramsay.[3] A magnetic field was applied in order to bring a particular transition into resonance with a laser line. As a result, the frequency of the dye laser had to be changed so as to follow the Zeeman shift of the electronic transition. The Zeeman effect for both the visible and infrared transitions was calculated with a set of preliminary molecular constants. The Zeeman components were easily identifiable in the laser excited fluorescence spectra even though their widths were Doppler broadened. It was not difficult for a transition with small N values such as $2_{20} \leftarrow 1_{10}$ to set the dye laser frequency on a particular Zeeman component of the transition within the Doppler width.

The search for double resonance signals was made by scanning either the magnetic field or the frequency of the dye laser. In the first method the frequency of the dye laser was set in resonance with a particular M_J component at a given magnetic field, and then the magnetic field was scanned around that value typically by ±500 G. Within the scan range, the dye laser was assumed to remain in resonance with that particular component within the Doppler width. The second method consisted of scanning the frequency of the dye laser, while the magnetic field was held fixed at some particular value, but, if necessary, the field was changed stepwise for each scan of the dye laser frequency. It occasionally happened that the magnetic field had to be changed over a range from a few kG up to 12 kG.

Figure 2 shows an example of the signals recorded by the first method (scanning the magnetic field) and with an intracavity cell; the frequency of the dye laser was not exactly set at the center of the Doppler profile of any hyperfine component. Two sets of triplets appeared

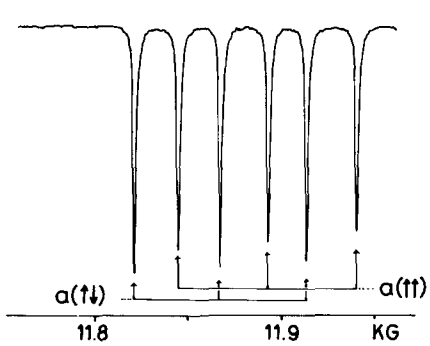

FIG. 2. Observed double resonance signal of $\tilde{A}(0, 10, 0)\ 1_{11} \leftarrow \tilde{A}(0, 9, 0)\ 2_{20}\ J$, $M_J = 1.5, -1.5 \leftarrow 1.5, -0.5$ transition by using the N_2O $P(28)$ laser line. The spectrum is obtained by scanning the magnetic field with an intracavity cell. The dye laser frequency is set to the $\tilde{A}(0, 9, 0)\ 2_{20} \leftarrow \tilde{X}(0, 0, 0)\ 1_{10}$, J, $M_J = 1.5, -0.5 \leftarrow 0.5, 0.5$ transition. The a (↑↑) shows the spectrum obtained by the copropagated infrared and optical radiations, and the a (↑↓) shows the spectrum by counterpropagated radiations.

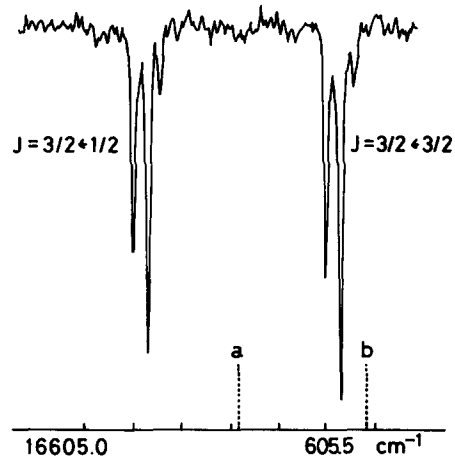

FIG. 3. Observed double resonance signal recorded by scanning the dye laser frequency with an extra-cavity cell. The infrared transition $\tilde{A}(0, 10, 0)\ 2_{11} \leftarrow \tilde{A}(0, 9, 0)\ 2_{20}\ J$, $M_J = 1.5, 0.5 \leftarrow 1.5, 1.5$ is in resonance with the CO_2 $P(6)$ laser line at the magnetic field of 4380 G. Higher and lower frequency spectra correspond, respectively, to the J, $M_J = 1.5, 1.5 \leftarrow 1.5, 0.5$ and J, $M_J = 1.5, 1.5 \leftarrow 0.5, 0.5$ components of the $\tilde{A}(0, 9, 0)\ 2_{20} \leftarrow \tilde{X}(0, 0, 0)\ 1_{10}$ transition. The dotted lines a and b show the positions of the $J = 1.5 \leftarrow 0.5$ and $J = 1.5 \leftarrow 1.5$ transitions at the zero field, respectively.

as expected for the para states of NH_2 (the resultant nuclear spin of the two protons I_H is zero). One set of the triplets was due to the interaction of molecules with the infrared and the visible lasers that were propagating to opposite directions, and the other set corresponded to the same propagation direction. The exact resonant fields were obtained by taking the average of the two corresponding components.

Figure 3 shows an example of the double resonance signals recorded as a function of the frequency of the dye laser with the magnetic field fixed at one of the infrared resonances (the second method). The cell was placed outside the laser cavity. As is expected, the spectrum is greatly simplified, in comparison with the ordinary laser excited fluorescence spectrum under the magnetic field. Double resonance was thus particularly useful in making assignments of M_J for the infrared transitions. One more notable point about the spectrum shown in Fig. 3 is the narrowing of the linewidth. It is about 150 MHz (HWHM), and the line shape is approximately Lorentzian. The lines were broadened by the large infrared power in the extra-cavity cell. The linewidth could be reduced to 70 MHz by placing the cell in the infrared laser cavity or by attenuating the infrared laser power. The hyperfine structures are resolved, but the splittings do not represent the "true" hyperfine splittings. A detailed discussion on the apparent hyperfine splitting and linewidth will be given in a later section.

One of interesting features of this experiment was the observation of transitions to unidentified levels that are most likely levels of a highly excited vibrational state in the ground electronic state. Figure 4 shows the Zeeman shifts of the $\Delta M_J = \pm 1$ components of the $\tilde{A}(0, 10, 0)2_{11} \leftarrow \tilde{A}(0, 9, 0)2_{20}$ infrared transition and the

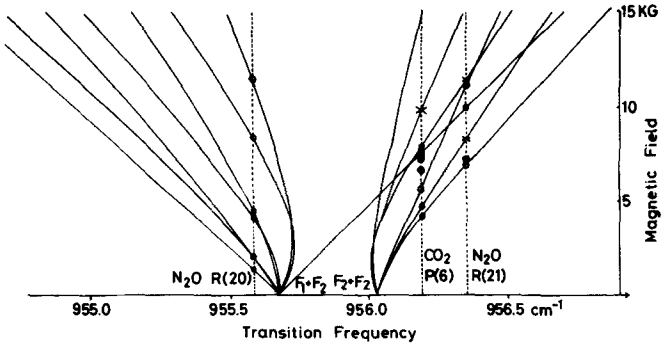

FIG. 4. Zeeman shift of the $\tilde{A}(0, 10, 0)\ 2_{11} \leftarrow \tilde{A}(0, 9, 0)\ 2_{20}$ transition with the $\Delta M = \pm 1$ selection rule. Small open circles indicate the observed resonances corresponding to increase in the total fluorescence intensity. The expected resonances marked by crosses were not observed. Solid circles show the unexpected resonances observed as decrease in the total fluorescence intensity.

CO_2 $P(6)$, N_2O $R(20)$, and N_2O $R(21)$ laser frequencies. This diagram was drawn at an intermediate stage of the analysis to make the assignment easier. Small open circles on Fig. 4 indicate the observed resonances. The expected resonances marked by crosses were, however, not observed in spite of very careful searches. Instead of them, additional unexpected resonances were found. They were reasonably strong, but were of opposite phase indicating a decrease in the total fluorescence intensity. When an interference filter ($\lambda_{center} = 568$ nm) with a width of 10 nm was used to eliminate fluorescence from the $\tilde{A}(0, 9, 0)$ levels, those additional lines were observed as a very slight increase of the fluorescence intensity. Their Zeeman shifts were found to be negative. It was reasonable to assume that the unexpected extra lines, hereafter referred to as the u lines, are associated with transitions to unknown states (hereafter called the u state); they were brought into crossing with the 2_{11} levels by the applied magnetic field.

III. INTERPRETATION OF OBSERVATIONS

The linewidths of the double resonance signals when the infrared transition was swept were found to be about 4 MHz, while those obtained by scanning the visible transition were about 70 MHz. As pointed out in a previous section, the hyperfine splittings of the IR signals were close to real splittings, whereas the corresponding hyperfine splittings of the visible transitions appeared to be much wider than the true splittings.

Figure 5 qualitatively explains how the linewidth and the hyperfine splitting of the double resonance signal are affected by the Doppler effect. The Doppler width (HWHM) of NH_2 at room temperature is 47 MHZ at 10 μm and 770 MHz at 16 600 cm^{-1}. When a visible transition with three hyperfine components is pumped by a single frequency dye laser, molecules with different M_I interact with the laser radiation when they have different velocities relative to the laser propagation directions. Because the Doppler width of the visible transition is much wider than the hyperfine separations, the numbers of pumped molecules for the three hyperfine components are almost the same. Therefore, the double resonance signal observed by sweeping the IR transition shows a triplet with almost equal intensities, as shown in Fig. 2. However, it should be noted that lines are Doppler

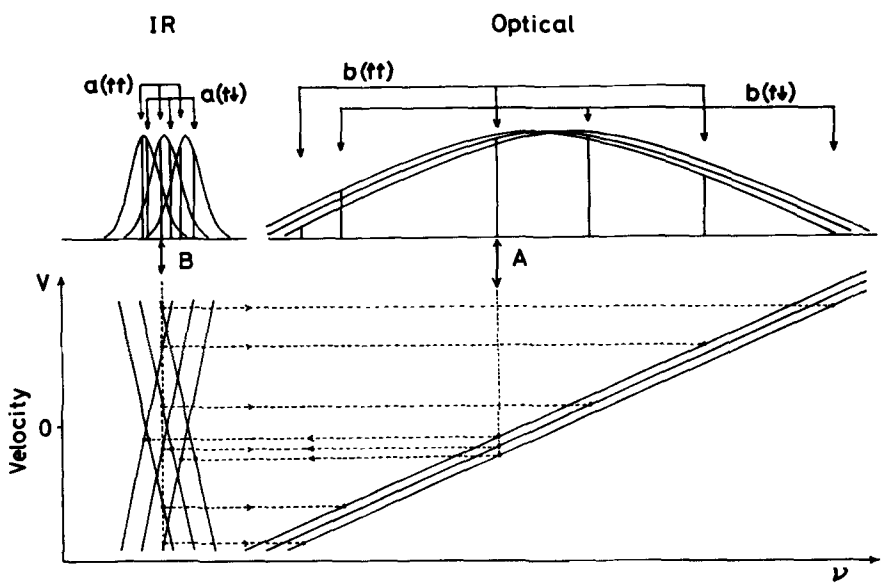

FIG. 5. The hyperfine structure and the linewidth observed by infrared–optical double resonance. The Doppler-broadened line profiles of infrared and optical transitions are shown on the top of the figure. Three profiles correspond to the $M_I = 1$, 0, and -1 components, respectively. The bottom part of this figure indicates the Doppler shift of the frequency $\nu = \nu_0\ (1 \pm v/c)$. The shifts are shown for both the IR radiations copropagated and counter-propagated to the optical radiation. The spectrum a shows the hyperfine structure of the IR transition observed by applying the dye laser pumping at the frequency indicated as A. The a(↑↑) is brought about by the interaction between the copropagated infrared and optical radiations, and the a(↑↓) is by counter-propagated radiations. The spectrum b corresponds to the otpical spectrum observed when the frequency of infrared laser pumping is set at the point B.

shifted and also the hyperfine separations do not exactly correspond to the true separations. When the signals are observed by sweeping the visible transition, the Doppler effect appears more conspicuously. In an example shown in Fig. 5, the hyperfine separations of the IR transition are comparable with the Doppler width, and, because the IR laser is considerably off-resonant from the center of the Doppler profile of the middle component of the hyperfine triplet, the highest-frequency hyperfine component located at the tail of the Doppler profile is barely resonant with the laser. As a result, the widely spaced hyperfine structures recorded by sweeping the frequency of the dye laser have intensities quite different from one another (see Fig. 3).

These situations can be understood more quantitatively using a detailed discussion, given in the Appendix. Equations (A6) and (A7) give the center frequencies of the infrared transition and the visible transition, respectively, on the double resonance. However, the infrared resonances were observed by sweeping the magnetic field rather than by sweeping the frequency. Equation (A6) must be modified, but the essential point is expressed by these equations. The ratio of k to k' is about 1/16, but, because $\omega_e - \omega_{21}$ can be of the order of a few hundred MHz, the "Doppler shift," i.e., the second term of Eq. (A6), becomes of the order of 10 MHz, which is comparable to the hyperfine splitting itself, as seen in Fig. 2. When the signal is recorded by sweeping the visible frequency, the Doppler shift is given by Eq. (A7). In this case, $\omega_r - \omega_{32}$ is about a few tens of MHz at most. However, because k'/k is about 16, the Doppler shift can be as large as a few hundred MHz. Therefore, the hyperfine structure shown in Fig. 3, is due mainly to that of infrared transition. Thus the observation of the signals with an intracavity cell is essential in obtaining the true hyperfine splitting of the infrared transition, because it allows us to observe two sets of lines Doppler shifted in opposite directions and to cancel out the second term of Eq. (A6) by taking their average.

From Eq. (A2), the linewidth of a line observed by sweeping the visible laser is given by

$$\Delta\omega_e = \frac{k+k'}{k}\Gamma \approx \frac{k'}{k}\Gamma ,$$

i.e., the width is about 16 times larger than the homogeneous width. On the other hand, the linewidth of an infrared signal is given by

$$\Delta\omega_r = \frac{k+k'}{k'}\Gamma \approx \Gamma ,$$

i.e., it is almost equal to the homogeneous width. The relative peak intensities among the hyperfine components are determined by the exponential factor in Eq. (A2).

IV. ANALYSIS AND RESULTS

The present paper reports the analysis of the $2_{11} - 2_{20}$, $u - 2_{20}$, and $1_{11} - 2_{20}$ transitions obtained by the excitation of $\tilde{A}(0, 9, 0)2_{20} - \tilde{X}(0, 0, 0)1_{10}$ transition. The observed resonances and their assignments are listed in Table I. The rotational states involved in these transitions belong to the para modification ($I_H = 0$). Therefore, only the interactions due to the nitrogen nucleus need to be considered. As the observed hyperfine structure of each M_J component listed in Table I is in the strong field case, M_I is a good quantum number and the selection rule for M_I is $\Delta M_I = 0$. The averages of the hyperfine splittings between the $M_I = 1$ and 0 and between the $M_I = 0$ and -1 components are shown in Table I.

A preliminary least-squares analysis without considering the interaction between the u state and the 2_{11} state resulted in a rather poor fit. In the least-squares fitting, it was found that all Zeeman components from the 2_{11} F_2 level ($J = 1.5$) were shifted toward lower energy, as the magnetic field was increased, as well as the $M_J = 2.5$ component from the 2_{11} F_1 level ($J = 2.5$). These observations indicate that a perturbing state exists which is higher in energy than the 2_{11} F_2 level and its rotational quantum number N is 3. We assumed that the perturbing state is the u level observed by the CO_2 $P(6)$ and N_2O $R(21)$ laser lines. This assumption is consistent with the Zeeman coefficients observed for the u line and also explains the absence of the resonances marked by crosses in Fig. 4. Because the quantum number M_J of the u level could be determined by scanning the dye laser frequency, we have established that the u state is an inverted doublet (F_1 lies lower than F_2).

The analysis was carried out using the following Hamiltonian:

$$H = \gamma \cdot N \cdot S + H_{\mathrm{HFS}} + H_Z + H_P , \qquad (1)$$

where γ is the effective spin-rotation coupling constant. The matrix elements of the hyperfine (H_{HFS}) and the Zeeman (H_Z) Hamiltonians were evaluated using decoupled functions $|N, K_a, S, J, M_J, I, M_I\rangle$ as bases.[22] The Zeeman operator H_Z includes the anisotropic g-factors $T_0^0(g_l)$, $T_0^2(g_l)$ and the rotational g-factors $T_0^0(g_r)$, $T_0^2(g_r)$ in addition to the isotropic spin g-factor g_s. The last term H_P is an interaction between the F_2 component of the u state and the F_1 of the 2_{11} state, i.e.,

$$V = \langle 2_{11},\ J = 2.5 \,|H_P|\, u(N = 3),\ J = 2.5\rangle .$$

The eigenvalues for the 2_{11} and u states were calculated by diagonalizing the 4×4 matrix, whereas for the 1_{11} and 2_{20} states 2×2 matrices needed to be solved. The matrix elements with $\Delta N = \pm 1$ were neglected and $\Delta N = 0$, $\Delta K = \pm 2$ matrix elements were taken into account only in the case of $K_a = 1$.

The least-squares fit was made in two steps. The first step, where only the $M_I = 0$ components were included, determined the molecular constants such as the g factors, the spin-rotation splittings, the interaction term between the u and 2_{11} states, and the zero-field infrared transition frequencies. At an intermediate stage, different sets of g factors were assumed for each rotational state in the upper state (1_{11}, 2_{11}, and u). As a result, a slightly better fit was attained, but the parameters themselves were determined less accurately because of the correlations among the g factors. The final fit was made by assuming the same g factors for the 1_{11}, 2_{11}, and u states, although it was questionable

TABLE I. Infrared optical double resonance spectra of NH_2.[a]

Laser line	$N_{K_aK_c}$	Transition[b] J	M_J	Field (Gauss)	a_N[c] (Gauss)	Δ[d] (MHz)
CO_2 $P(6)$[e]	$2_{11} \leftarrow 2_{20}$	1.5 ← 1.5	0.5 ← 1.5	4370	35	−19
			−0.5 ← 0.5	4912	47	−1
			−1.5 ← −0.5	6072	79	1
		2.5 ← 1.5	2.5 ← 1.5	7575	50	4
		1.5 ← 1.5	1.5 ← 0.5	8217	41	−25
			1.5 ← 1.5	5704	32	−6
			0.5 ← 0.5	6339	39	0
			−1.5 ← −1.5	12340	135	−5
N_2O $R(21)$	$2_{11} \leftarrow 2_{20}$	1.5 ← 1.5	0.5 ← 1.5	7198	35	18
		2.5 ← 1.5	2.5 ← 1.5	10111	51	−10
		1.5 ← 1.5	−1.5 ← −0.5	11543	78	−6
			1.5 ← 1.5	8497	37	12
N_2O $R(20)$	$2_{11} \leftarrow 2_{20}$	2.5 ← 1.5	−2.5 ← −1.5	1066	50	8
			−0.5 ← −1.5	1744	43	8
			−1.5 ← −0.5	1807	54	9
			0.5 ← −0.5	3597	41	10
			−0.5 ← 0.5	3979	55	2
			1.5 ← 0.5	7788	60	2
			0.5 ← 1.5	10446	67	−5
N_2O $R(26)$	$2_{11} \leftarrow 2_{20}$	2.5 ← 2.5	1.5 ← 2.5	6191	48	3
			0.5 ← 1.5	7092	44	1
			−0.5 ← 0.5	8926	46	1
			1.5 ← 0.5	12171	55	0
			−1.5 ← −0.5	13252	53	−15
			1.5 ← 1.5	8268	51	8
			0.5 ← 0.5	10414	46	−7
N_2O $R(27)$	$2_{11} \leftarrow 2_{20}$	1.5 ← 2.5	−1.5 ← −2.5	337[f]	62	
			−0.5 ← −1.5	634[f]	63	
			−1.5 ← −0.5	634[f]	63	
			−0.5 ← 0.5	2325	67	−5
			1.5 ← 0.5	6830	41	16
			−1.5 ← −1.5	455	67	−19
			−0.5 ← −0.5	1078	66	−3
			0.5 ← 0.5	4324	41	4
N_2O $R(28)$	$2_{11} \leftarrow 2_{20}$	1.5 ← 2.5	−1.5 ← −2.5	8497	56	6
			−0.5 ← −1.5	11095	50	1
			−1.5 ← −0.5	13298	61	−3
			−1.5 ← −1.5	10385	56	10
			−0.5 ← −0.5	14213	50	0
CO_2 $P(6)$[e]	$u \leftarrow 2_{20}$	3.5 ← 1.5	−1.5 ← −0.5	7337	16	19
			−0.5 ← −1.5	6652	21	2
			−1.5 ← −1.5	5631	18	−15
N_2O $R(21)$	$u \leftarrow 2_{20}$	3.5 ← 1.5	0.5 ← −0.5	7104	24	−4
N_2O $P(26)$	$1_{11} \leftarrow 2_{20}$	0.5 ← 1.5	−0.5 ← 0.5	10276	36	−5
			0.5 ← 1.5	10520	60	5
N_2O $P(27)$	$1_{11} \leftarrow 2_{20}$	1.5 ← 1.5	1.5 ← 0.5	3940	45	−7
N_2O $P(28)$	$1_{11} \leftarrow 2_{20}$	1.5 ← 1.5	−0.5 ← −1.5	11770	48	2
			−1.5 ← −0.5	11880	47	4
N_2O $P(22)$	$1_{11} \leftarrow 2_{20}$	1.5 ← 2.5[g]		0		

[a] All resonances were obtained by the excitation of the $\tilde{A}(0, 10, 0)$ $2_{20} \leftarrow \tilde{X}(0, 0, 0)$ 1_{10} transition.
[b] The vibronic transition is $\tilde{A}(0, 10, 0) \leftarrow \tilde{A}(0, 9, 0)$ except for the $u \leftarrow 2_{20}$ transitions.
[c] a_N is the average of the observed nitrogen hyperfine splittings.
[d] Δ = calc. − obs. .
[e] 10.6 μm band.
[f] Not included in the least-squares analysis.
[g] This transition coincides with the laser line within the Doppler width.

to assume that the g factors for the u state were the same as in the 2_{11} state.

In the second step, the hyperfine interaction constants were determined by minimizing the difference between

TABLE II. Molecular constants of NH_2.[a]

	$(0, 10, 0)2_{11}$	u	$(0, 10, 0)1_{11}$	$(0, 9, 0)2_{20}$
γ	−4084.0(42)	−7282(69)	−15501(12)	−57342.5(23)
$g_s - T_0^0(g_l)/\sqrt{3}$	1.994 70(62)	b	b	1.996 3(19)
$T_0^2(g_l)$	−0.024 2(31)	b	b	−0.027 7(46)
$T_0^0(g_r)$	0.008 95(57)	b	b	0.050 85(60)[c]
$T_0^2(g_r)$	−0.011 5(18)	b	b	···
$E(cm^{-1})$	958.681 2(2)	959.7295(29)	918.0598(3)	0.0
V	4124(62)			
σ_{FC}	147.64(70)	10.9(48)	d	146.48(96)
T_{aa}	···	−38(23)	···	−60.5(21)
T_{bb}	74.0(24)	···	d	···

[a]In MHz except for g factors and E. Values in parentheses denote a standard deviation and apply to the last digits of the constants. The rotational quantum numbers of the u level are assumed to be 3_{30}, see the text.
[b]Assumed to be equal to the constants in the $(0, 10, 0)2_{11}$ state and fixed.
[c]This value is $T_0^0(g_r) - T_0^2(g_r)/\sqrt{2}$.
[d]The same parameters as in the $(0, 10, 0)2_{11}$ state are used.

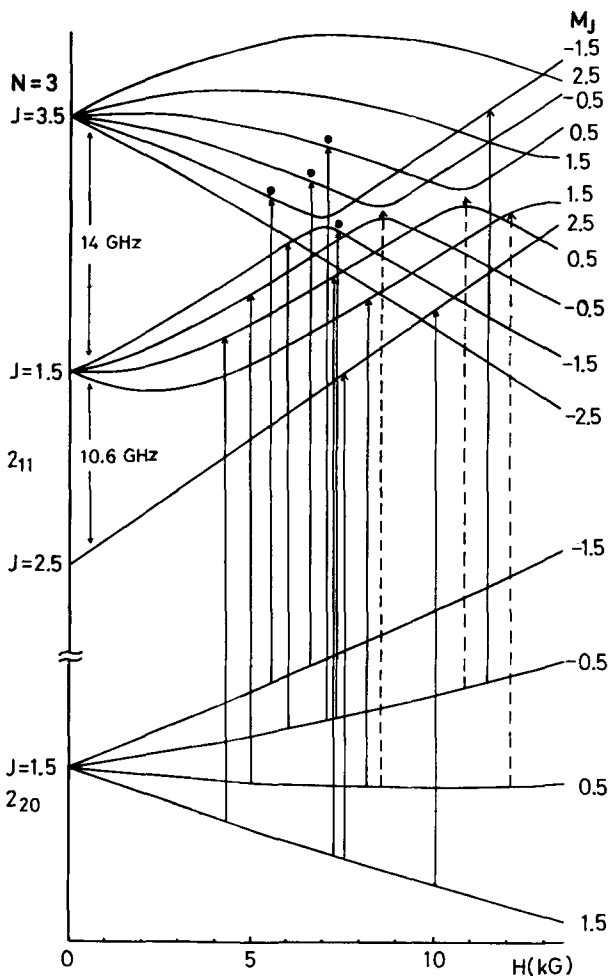

FIG. 6. Zeeman energy levels of u $N=3$ F_1, $\tilde{A}(0, 10, 0)$ 2_{11}, and $\tilde{A}(0, 9, 0)$ 2_{20} F_2 states. Zeeman shifts were calculated by considering the interaction between the u and $(0, 10, 0)$ 2_{11} levels. The full lines indicate the transitions observed by using the CO_2 $P(6)$ and N_2O $R(21)$ laser lines with $\Delta M = \pm 1$ polarization (except for a u line which was observed with $\Delta M = 0$ polarization). The broken lines correspond to the crosses in Fig. 4. The observed four u lines are marked by solid circles.

the calculated and observed hyperfine splittings, where the assignments and other parameters derived by the first step were employed. The MODR results on the 2_{11} state by Hills and Curl[23] were included in the fit. The determined molecular constants are listed in Table II.

Figure 6, which was drawn using the final molecular constants, shows the interaction between the u state and the 2_{11} state. It should be noted here that, although only states of the same J interact with each other at zero field, the Zeeman effect causes mixing between states of $\Delta J = \pm 1$ so that the level anticrossings appear, as shown in Fig. 6.

V. DISCUSSION

The observed u state in the present work was shown to have $N=3$ with the F_1 component being lower than the F_2 component (i.e., an inverted doublet). However, the vibrational assignment of the u state could not be made from the present observation alone, and even the K_a and K_c quantum numbers were not uniquely determined. Because the fluorescence yield from the u level was quite small, the u level perhaps belongs to a higher vibrational state of the ground state, like a level found by Hills and Curl from microwave optical double resonance,[13,16] or to a vibrational state in the $\tilde{A}$ electronic state with v_1 and/or v_3 different from zero. The rovibronic symmetry species of the u state must be A_2 in order to interact with $(0, 10, 0)2_{11}$ in the excited $\tilde{A}$ electronic state. Therefore, if the u state belongs to a vibrational state of the ground electronic state with an even v_3 quantum number, the rotational state must be either 3_{30} or 3_{12}, and if it is in an odd v_3 state, the rotational state must be 3_{22}. As to the latter possibility, no appropriate level could be found near the $(0, 10, 0)2_{11}$ level within the $\tilde{A}$ electronic state mainfold, when the results of Dressler and Ramsay[3] were employed.

The vibrational assignment for the u state was in-

ferred by using the fundamental frequencies of the ν_1 and ν_3 vibrations recently determined through an analysis of absorption spectra recorded with a difference-frequency laser in the 3 μm region[24] and the term values reported by Jungen, Hallin, and Merer[25] for the higher excited states of the ν_2 vibration and by assuming that the anharmonicity of H_2O[26] was applicable to NH_2. The vibrational term values were derived to be 17478, 17519, and 17566 cm^{-1} for $K_a=1$, 2, and 3, respectively, by subtracting $B[N(N+1)-K_a^2]$ from the observed term value of u, 17598.96 cm^{-1}. The calculated term value that is the closest to these values is 17578 cm^{-1} obtained for the $\tilde{X}(2, 8, 0)K_a=3$ vibronic state. However, the analysis by Jungen, Hallin, and Merer[27] revealed that the spin-orbit coupling constant in the $\tilde{X}(0, 8, 0)$ vibronic state was -11.605 cm^{-1}, whereas the spin splitting determined from our analysis was -0.8499 cm^{-1}.

The hyperfine coupling constants in the $\tilde{A}(0, 9, 0)2_{20}$ state obtained in the present work are consistent with the values derived by Dixon and Field[20] for the same state from an analysis of the level crossing spectrum. Their value of $\sigma_{FC}-T_{bb}/7$ is 122.4 MHz, which may be compared with the present result 129.2(1.1) MHz.

The analysis of hyperfine structures of the u lines that showed small splittings compared with those of other "normal" lines has been carried out by assuming the rotational quantum numbers of u level to be 3_{30}. As shown in Table II, the values of σ_{FC} and T_{bb} thus obtained are close to those in the $\tilde{X}(0, 0, 0)$ state obtained by Cook *et al.*[14] using microwave optical double resonance: $\sigma_{FC}=28.2(0.6)$ MHz, $T_{aa}=-42.8(1.8)$ MHz, $T_{bb}=-44.8(1.4)$ MHz, and $T_{cc}=87.5(0.8)$ MHz. Therefore, the u level is very likely to be in the $\tilde{X}$ state rather than in the $\tilde{A}$ state.

As the relation $T_{bb}=-2T_{aa}$ can be assumed in the $\tilde{A}$ state (σ radical), the T_{bb} value differs considerably in the $\tilde{A}(0, 10, 0)2_{11}$ and $\tilde{A}(0, 9, 0)2_{20}$ state. However, in order to discuss this interesting change, we need more data on T_{bb} in other vibrational and rotational levels of the $\tilde{A}$ state. Further studies along this line are being made at the Institute for Molecular Science.

In summary, we have presented for the first time, an example of infrared–optical double resonance spectroscopy combined with magnetic field tuning, i.e., laser magnetic resonance spectroscopy in excited electronic states. We believe this new spectroscopic method is suitable for high-resolution observations of infrared transitions of stable molecules as well as transient species in excited electronic states.

We can obtain detailed molecular constants, including g factors, spin splittings and hyperfine coupling constants, for the levels concerned. Furthermore, this technique provides some useful information about a level in the other vibronic state, the u state, which has interactions with the $\tilde{A}$ electronic state. Observations of the levels in such u states have been reported by some studies on ordinary absorption spectroscopy, laser excitation spectroscopy, and the MODR method. However, assignment of rotational quantum number is not straightforward in these spectroscopic methods. The present method IODR can easily afford partial rotational quantum numbers as well as separations of spin splittings from an analysis the Zeeman shift of each M_J component.

A more interesting feature of this IODR method is the determination of the interaction term V between the electronic state concerned and the other state, presumably, a highly excited vibrational level of the ground electronic state. The V term, mainly due to electronic Coriolis interaction and spin-orbit interaction,[27] mixes these electronic states so that it opens a path for quenching of the fluorescent level. This means that the V term is very important for understanding how radiative lifetime change for each rotational level.

ACKNOWLEDGMENTS

We wish to thank Dr. G. W. Hills, Dr. R. F. Curl, Jr., and Dr. J. M. Brown for informing us of their microwave–optical double resonance data prior to publication. The present work was supported by the joint studies program (1978–1979) of the Institute for Molecular Science. Calculations in this work were carried out at the Computer Center of the Institute for Molecular Science.

APPENDIX

Let us consider a typical three-level system shown in Fig. 7. Suppose the fluorescence from level three is detected. The electric field of the laser radiation is expressed as

$$E(t, z)=\epsilon_r^{(+)}\exp[i(\omega_r t+kz)]+\epsilon_r^{(-)}\exp[i(\omega_r t-kz)] + \epsilon_e\exp[i(\omega_e t-k'z)]+\text{c.c.}\,, \quad \text{(A1)}$$

where $\epsilon_r^{(\pm)}$ and ϵ_e are the electric field intensities for the infrared and the visible lasers, and k and k' are defined by $k=\omega_r/c$ and $k'=\omega_e/c$. The ordinary perturbation calculation using the density matrix equation gives the dominant term of the population change of level three produced by the double resonance process as

$$\Delta N_3=\frac{4\sqrt{\pi}N_1^{(0)}|x_r^{\pm}|^2|x_e|^2(k+k')\Gamma}{\gamma^2 u[(k'\Delta\pm k\delta)^2+(k+k')^2\Gamma^2]}\exp[-\delta^2/(k'u)^2], \quad \text{(A2)}$$

where Δ and δ are defined by

$$\Delta=\omega_{32}-\omega_r\,, \quad \text{(A3)}$$

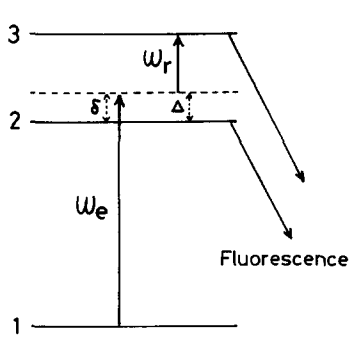

FIG. 7. Three-level system in infrared–optical double resonance.

$$\delta = \omega_s - \omega_{21} \ . \tag{A4}$$

In Eq. (A2), $x_r^{\pm}$ and x_s are the Rabi frequencies defined by $x_r^{\pm} = \mu_{23}\epsilon_r^{\pm}/\hbar$ and $x_s = \mu_{12}\epsilon_s/\hbar$. The mean velocity of the molecules is denoted by u, and Γ and γ are the polarization relaxation rate and the population relaxation rate, respectively. Equation (A2) expresses the line shape function; the positive sign in Eq. (A2) applies to the lines observed when the visible and the infrared laser proceed in opposite directions, and the negative sign to cases where both the lasers travel to the same direction. The center frequency of the line is given by

$$k'\Delta \pm k\delta = 0 \ , \tag{A5}$$

i.e.,

$$\omega_r = \omega_{32} \pm k/k'(\omega_s - \omega_{21}) \ , \tag{A6}$$

or

$$\omega_s = \omega_{21} \pm k'/k(\omega_r - \omega_{32}) \ . \tag{A7}$$

[1] I. P. Herman, A. Javan, and R. W. Field, J. Chem. Phys. **68**, 2398 (1978).
[2] B. J. Orr and G. F. Nutt, J. Mol. Spectrosc. **84**, 272 (1980).
[3] K. Dressler and D. A. Ramsay, Philos. Trans. R. Soc. London Ser. A **251**, 553 (1959).
[4] J. W. C. Johns, D. A. Ramsay, and S. C. Ross, Can. J. Phys. **54**, 1804 (1976).
[5] F. W. Birss, D. A. Ramsay, S. C. Ross, and C. Zauli, J. Mol. Spectrosc. **78**, 344 (1979).
[6] M. Vervloet, M. F. Merienne-Lafore, and D. A. Ramsay, Chem. Phys. Lett. **57**, 5 (1978).
[7] M. Kroll, J. Chem. Phys. **63**, 319 (1975).
[8] M. Vervloet and M. F. Merienne-Lafore, J. Chem. Phys. **69**, 1257 (1978).
[9] M. Vervloet, thesis, Reims, 1978.
[10] J. B. Halpern, G. Hancock, M. Lenzi, and K. H. Welge, J. Chem. Phys. **63**, 4808 (1975).
[11] P. B. Davies, D. K. Russell, B. A. Thrush, and H. E. Radford, Proc. R. Soc. London Ser. A **353**, 299 (1977).
[12] G. W. Hills, J. M. Cook, R. F. Curl, and F. K. Tittel, J. Chem. Phys. **65**, 823 (1976).
[13] G. W. Hills and R. F. Curl, J. Chem. Phys. **66**, 1507 (1977).
[14] J. M. Cook, G. W. Hills, and R. F. Curl, J. Chem. Phys. **67**, 1450 (1977).
[15] G. W. Hills, R. S. Lowe, J. M. Cook, and R. F. Curl, J. Chem. Phys. **68**, 4073 (1978).
[16] R. S. Lowe, J. V. V. Kasper, G. W. Hills, W. Dillenschneider, and R. F. Curl, J. Chem. Phys. **70**, 3356 (1979).
[17] K. Kawaguchi, C. Yamada, E. Hirota, J. M. Brown, J. Buttenshaw, C. R. Parent, and T. J. Sears, J. Mol. Spectrosc. **81**, 60 (1980).
[18] F. W. Birss, M. F. Merienne-Lafore, D. A. Ramsay, and M. Vervloet, J. Mol. Spectrosc. **85**, 493 (1981).
[19] G. W. Hills, D. L. Philen, R. F. Curl, and F. K. Tittel, Chem. Phys. **12**, 107 (1976).
[20] R. N. Dixon and D. Field, Mol. Phys. **34**, 1563 (1977).
[21] M. Kakimoto, S. Saito, and E. Hirota, J. Mol. Spectrosc. **80**, 334 (1980).
[22] J. M. Brown and T. J. Sears, Mol. Phys. **34**, 1595 (1977).
[23] G. W. Hills and R. F. Curl (private communication).
[24] T. Amano, P. F. Bernath, and A. R. W. McKellar (unpublished).
[25] Ch. Jungen, K. E. J. Hallin, and A. J. Merer, Mol. Phys. **40**, 25 (1980).
[26] G. Herzberg, *Infrared and Raman Spectra of Polyatomic Molecules* (Van Nostrand, Princeton, 1945).
[27] Ch. Jungen, K. E. J. Hallin, and A. J. Merer, Mol. Phys. **40**, 65 (1980).